

Graphite edge controlled registration of monolayer MoS₂ crystal orientation

Chun-I Lu,¹ Christopher John Butler,¹ Jing-Kai Huang,² Cheng-Rong Hsing,² Hung-Hsiang Yang,¹ Yu-Hsun Chu,¹ Chi-Hung Luo,¹ Yung-Che Sun,¹ Shih-Hao Hsu,¹ Kui-Hong Ou Yang,¹ Ching-Ming Wei,^{2,a)} Lain-Jong Li,^{2,b)} and Minn-Tsong Lin^{1,2,c)}

¹Department of Physics, National Taiwan University, Taipei 10617, Taiwan

²Institute of Atomic and Molecular Sciences, Academia Sinica, Taipei 10617, Taiwan

(Received 25 January 2015; accepted 24 April 2015; published online 7 May 2015)

Transition metal dichalcogenides such as the semiconductor MoS₂ are a class of two-dimensional crystals. The surface morphology and quality of MoS₂ grown by chemical vapor deposition are examined using atomic force and scanning tunneling microscopy techniques. By analyzing the moiré patterns from several triangular MoS₂ islands, we find that there exist at least five different superstructures and that the relative rotational angles between the MoS₂ adlayer and graphite substrate lattices are typically less than 3°. We conclude that since MoS₂ grows at graphite step-edges, it is the edge structure which controls the orientation of the islands, with those growing from zig-zag (or armchair) edges tending to orient with one lattice vector parallel (perpendicular) to the step-edge. © 2015 Author(s). All article content, except where otherwise noted, is licensed under a Creative Commons Attribution 3.0 Unported License.

[<http://dx.doi.org/10.1063/1.4919923>]

Molybdenum disulfide (MoS₂), a layered semiconductor whose layers are weakly bound by the van der Waals force,^{1–4} has a great potential for application in electronic devices. Recently, many proposed novel devices are based on heterostructures of MoS₂ and graphene.^{5–9} Such heterostructures offer the possibility to create devices with new functionalities or better performance in electronic logic and memory devices,^{9–11} and also offer great potential in the hydrogen evolution reaction.¹² Graphene/MoS₂ heterostructures have also been adopted to demonstrate an extremely high photosensitivity and gain¹³ as well as the ultrasensitive detection of DNA hybridization.¹⁴ Hence, the study of the interfaces between MoS₂ and graphene (or graphite) is critically important and may provide useful hints for various applications.^{6,15} Shi *et al.* have recently reported the formation of MoS₂ flakes on the graphene surface via thermal decomposition of ammonium thiomolybdate.¹⁶ Although there is a large lattice mismatch between the MoS₂ and the graphene structure, graphene can serve as an epitaxial substrate for MoS₂. The results encourage the fundamental exploration of the interaction between MoS₂ and hexagonal graphene or graphite.

In this work, we perform atomic force microscopy (AFM) and scanning tunneling microscopy (STM) measurements on sub-monolayer chemical vapor deposition (CVD) grown MoS₂ on a substrate of highly oriented pyrolytic graphite (HOPG).^{17,18} The CVD process, as opposed to solution transfer used in previous reports, can prevent contaminations such as trapped water at the interface.¹⁹ MoS₂ grown using the CVD method has previously been investigated using STM and photoluminescence techniques,²⁰ but the detailed atomic scale structure at the CVD MoS₂/HOPG interface has not yet been elucidated. We find that the

triangular islands are atomically clean and defect-free, and that clear moiré patterns can be observed, which in general arise due to a lattice mismatch or rotational mis-alignment between a weakly interacting adlayer and substrate.²¹ By analyzing the atomic lattice and moiré pattern, the stacking orientation between the MoS₂ adlayer and the HOPG substrate can be obtained. We find that there exist at least five possible orientations of MoS₂ islands with respect to the HOPG substrate lattice. An investigation of the superstructure dependent surface energy using *ab initio* calculations indicates that inter-layer interactions are not sufficient to impose such a constraint on the MoS₂ islands' lattice orientation. However, we find that the MoS₂ islands show a preference for forming with a small relative angle of rotation with respect to the substrate, with angles above a few degrees found to be rare. As *ab initio* calculations indicate that the difference in surface energy for different orientations is insufficient to explain this tendency, we instead construct a simple model attributing it to the type of graphite edge (zig-zag or armchair) at which islands nucleate. These findings offer a microscopic explanation for the apparently ordered orientations of micron sized MoS₂ islands as observed in AFM images.

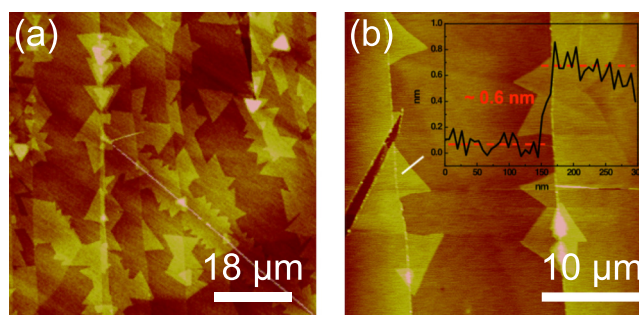


FIG. 1. AFM morphology of CVD-grown islands of MoS₂ deposited on an HOPG surface. (a) $70 \times 70 \mu\text{m}^2$ and (b) $30 \times 30 \mu\text{m}^2$, at another region of the sample. The inset shows the line profile taken along the white line in (b).

^{a)}Electronic mail: cmw@phys.sinica.edu.tw

^{b)}Electronic mail: lanceli@gate.sinica.edu.tw

^{c)}Electronic mail: mtlin@phys.ntu.edu.tw

The micrometer-scale AFM morphology of sub-monolayer MoS₂ on HOPG is shown in Fig. 1. The HOPG substrate's step-terrace morphology is overlaid by triangular MoS₂ thin film islands. Most of these triangles form across an HOPG step, or in contact with the step at one of their edges. Also of interest is the ordered orientation of the islands. Toward the left hand side of Fig. 1(a), the majority of islands are aligned roughly with one corner pointing along the step edge, and one side perpendicular to it. Fig. 1(b) shows MoS₂ islands arranged on a pair of HOPG step edges in another sample location, with the profile taken along the white line indicating a single layer height of around 0.6 nm. Here, it is seen that the islands tend to align with one side against the HOPG edge, and one corner pointing at a near-perpendicular angle to it. This suggests that the apparent order is determined by detailed properties of the substrate, such as the relative orientation between the HOPG edges and surrounding surface lattice, which vary between different regions, but which provide common conditions controlling the growth orientation of separate islands in close proximity.

Fig. 2(a) shows a high resolution STM image taken on an MoS₂ island, using $V_{bias} = -1$ V. The hexagonal surface lattice corresponds to the outermost layer of S atoms of the MoS₂ monolayer. As well as the periodicity of the atomic lattice, a hexagonal moiré pattern is also observed. Fig. 2(b) shows the STM image scanned in the same region as Fig. 2(a), but with $V_{bias} = -0.1$ V, within the band gap of MoS₂, and a current set-point of 50 nA. Interestingly, a different surface lattice is now seen, with a lattice length of 0.246 nm,¹⁷ consistent with the lattice constant of graphite.²¹ This difference in apparent morphology is attributed to a change in the source of electrons tunneling to the STM tip. A bias voltage of $V_{bias} = -1$ V draws a tunnel current from the MoS₂ valence band, whereas a bias of $V_{bias} = -0.1$ V, within semiconductor band gap, should yield almost no contribution from the MoS₂. Instead, the STM tip descends to probe metallic HOPG bands in order to satisfy the tunneling current set-point, while the MoS₂ layer is effectively electronically transparent at this energy. Tunneling spectra acquired on the

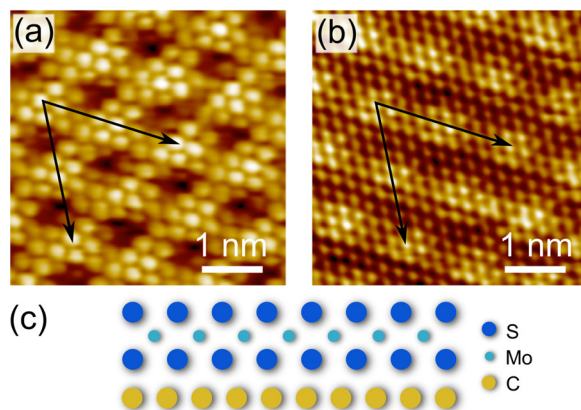


FIG. 2. STM atomic resolution images taken on an MoS₂ island. (a) 4.3×4.3 nm², $V_{bias} = -1$ V, and $I_{set} = 10$ nA. The lattice constant measured is 0.315 ± 0.001 nm. (b) 4.3×4.3 nm², $V_{bias} = -0.1$ V, and $I_{set} = 50$ nA. An atomic lattice with a lattice constant of 0.246 nm is now seen. The black arrows label the superstructure period. (c) A schematic diagram shows the side view projected along the superstructure lattice vector of length 7 times the MoS₂ lattice vector and 9 times that of HOPG.

MoS₂ island are shown in the supplementary material.¹⁷ Because the HOPG provides the majority of the tunnel current in the latter case, the apparent morphology in the constant current image corresponds to that of the HOPG, rather than the MoS₂ adlayer. In this way, the atomic lattice of the substrate can be observed directly rather than by inference based on measurements of nearby regions of bare substrate. This powerful technique could in principle be generalized to many heterostructure systems in which a thin semiconducting film overlays a metallic substrate or even a semiconducting substrate, provided there is a suitable mis-alignment of band edges between the substrate and adlayer.

Instead of the apparent periodicity of the moiré pattern, we identify a larger unit cell which more correctly characterizes the surface superstructure.¹⁷ In the case of the moiré pattern shown in Fig. 2, we describe the superstructure with unit cells containing four moiré peaks, though in general the proper superstructure unit cell may contain any integer number of moiré peaks. Fig. 2(c) shows the schematic diagram of the side view projected along the lattice vectors of this new unit cell (indicated by the black arrows in Figs. 2(a) and 2(b)). The lattice constant of MoS₂ in Fig. 2(a) is measured to be 0.315 ± 0.001 nm, and in Fig. 2(b) the HOPG lattice parameter is 0.246 nm. The suitable superstructure for this system is thus $(0.315 \pm 0.001 \text{ nm}) \times 7 = 2.205 \pm 0.007$ nm, which matches $0.246 \text{ nm} \times 9 = 2.214$ nm, over which distance the MoS₂ and HOPG lattices fall out of registry and then back into registry with each other.

In general, moiré superstructures can be formed either by a lattice mismatch between two lattices whose lattice vectors are aligned, by a relative rotation between two layers with equal lattice parameters, or by some combination of these two effects. The MoS₂ island shown in Fig. 2 represents the former case, in which there is no relative rotation, and the pattern arises purely from the fixed lattice mismatch. The superstructure is characterized as R(49/81), meaning the superstructure lattice parameters are $\sqrt{49}$ times the MoS₂ lattice constant, and $\sqrt{81}$ times the HOPG lattice constant. In general, however, lattice rotation in MoS₂ islands is also possible, and controls the periodicity of the resulting moiré superstructure. As moiré periodicity varies strongly with inter-lattice angle, even a narrow distribution of angles leads to a broad distribution of Bragg peaks, which is unlikely to be resolved using an area-averaging technique such as Low-Energy Electron Diffraction (LEED). In order to investigate the distribution of relative rotation between the MoS₂ adlayer island and the HOPG substrate, we perform a survey of MoS₂ islands by STM. Various moiré patterns are observed in a collection of high-resolution STM images and classified according to the scheme outlined above and demonstrated in Fig. 2.

Although the superstructure lattice vectors are not parallel with those of the atomic lattice, the periodicity can still be interpreted using the basis expansion of the unit cell vectors of MoS₂ or HOPG. For Fig. 3(a), beyond the moiré pattern period, a repeating superstructure can be found and labeled as R(37/61). The superstructure periodicity is characterized by a unit cell composed of $3\mathbf{i} + 4\mathbf{j}$ or equivalently $4\mathbf{I} + 5\mathbf{J}$, where the unit-vectors (\mathbf{i}, \mathbf{j}) are the lattice vectors of MoS₂ and (\mathbf{I}, \mathbf{J}) are those of HOPG. From this information,

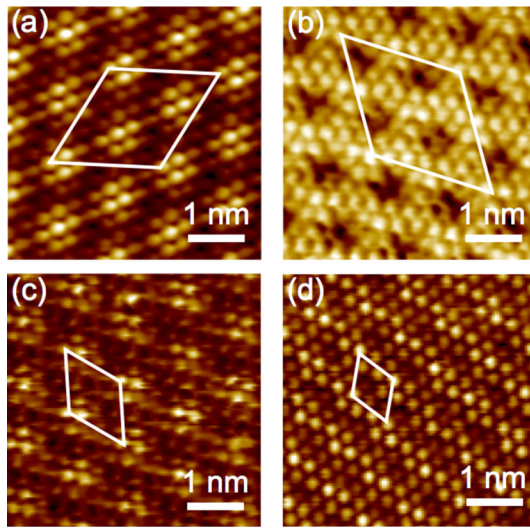


FIG. 3. Beside the R(49/81) case, other moiré superstructures can also be found: (a) R(37/61), imaged using a bias voltage of -0.2 V, and a tunneling set-point of 5 nA, (b) R(43/73), -1 V, 1 nA, (c) R(13/21), -1 V, 10 nA, and (d) R(7/12), -0.5 V, 0.5 nA. In each figure, the white rhombus indicates the suitable superstructure unit cell.

even without observation of the substrate lattice, we can retrieve information about the orientation of the underlying layer and obtain the relative rotational angle θ by using trigonometry. Here, the angle θ between the two lattices is $\sim 1^\circ$. Using the same concept, the superstructures observed in Figs. 3(b)–3(d) can be labeled as R(43/73), R(13/21), and R(7/12), respectively. The corresponding relative angles θ are 2° , 3° , and 11° , respectively. The angles θ in these cases were confirmed by measuring the nearby bare HOPG surface. The lattice constants of these five cases are all in the range of 0.315 ± 0.002 nm. The details of the atomic structure and the relative rotational angle analysis are collected in the supplementary material.¹⁷

In order to elucidate the occurrence of different moiré patterns of MoS₂ on HOPG discovered using STM, we perform a theoretical investigation of the binding energies between the MoS₂ and graphene. Since the strain energy of the MoS₂ layer is known to be smaller than that of graphene,²² we use a supercell approach to model the system with two planar lattice unit vectors based on the graphene experimental lattice constant (0.2464 nm). The vacuum spacing, used to avoid the spurious interaction among neighboring cells, is 1.5 nm. Calculations were performed in the framework of density functional theory (DFT)^{23,24} using the local density approximation (LDA).²⁵ Fig. 4 lists the binding energies (per primitive cell of graphene) of five different superstructures R(n/m) observed in STM versus the lattice constant of the strained MoS₂ layer. The five binding energies show no significant variation within 2 meV. This indicates that the constraint on the orientations of MoS₂ islands does not originate chiefly from inter-layer interactions, and that the explanation for such a constraint must be sought elsewhere.

The atomic resolution STM images and the superstructure analysis offer some explanation as to why the MoS₂ islands have preferred orientations as shown in the AFM image in Fig. 1(a). Besides the five cases shown in Figs. 2

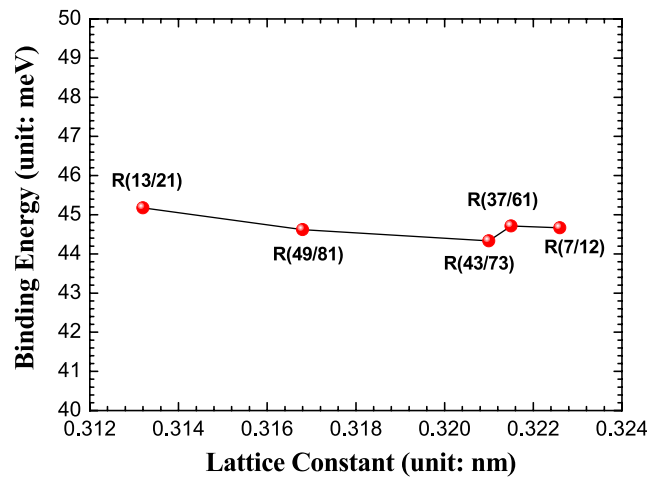


FIG. 4. DFT calculation of the binding energy for each of the superstructures shown in Figs. 2 and 3. In each case, the graphene lattice constant is fixed at 0.2464 nm. The MoS₂ lattice constant, under varying degrees of strain, is shown on the x-axis. The energies are seen to be similar within 2 meV.

and 3, we find that none of the twelve moiré patterns observed in our experiments correspond to angles greater than 11° , and that for most of them, the angle θ is smaller than 3° . For MoS₂ films prepared by transfer printing, we might expect a random distribution of rotations θ (between 0° and a maximum of 30°). However, for CVD grown MoS₂ studied in this work, a small angle θ may be enforced by the conditions in the early stages of nucleation and growth of each island. As islands typically form at the edges of an HOPG terrace, we must consider the type of HOPG edge (typically characterized as either a “zig-zag” or “armchair” edge) from which the MoS₂ island grows. Fig. 5 shows schematic representations of MoS₂ islands extending from zig-zag and armchair edges. Since a zig-zag edge is necessarily parallel with an HOPG lattice vector, in order that the lattice vectors of MoS₂ maintain a small angle θ with respect to the HOPG lattice vectors, one of the MoS₂ lattice vectors in the MoS₂ island growing from a zig-zag edge should remain parallel with the HOPG edge. On the other hand, an armchair edge has an angle of 30° with the HOPG lattice vectors. Hence, one of the lattice vectors of MoS₂ growing around an armchair edge should have an angle of around 30° with the HOPG edge, resulting in one of the corners of the MoS₂ island pointing along the HOPG edge. Looking back on the

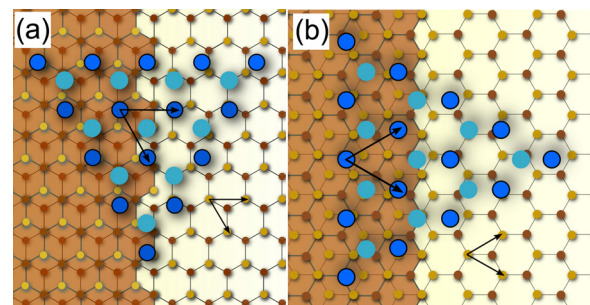


FIG. 5. Schematic diagrams of MoS₂ adlayer orientation on HOPG with (a) arm-chair edge or (b) zig-zag terrace substrate, in which the higher HOPG terrace is to the left, the blue dotted array are S atoms and the light-blue dotted array are Mo atoms (the lattice constants are not to scale).

AFM images presented in Fig. 1, we can now infer that the HOPG terraces shown in Fig. 1(a) likely have armchair edges, while those in Fig. 1(b) likely have zig-zag edges. In other words, the orientation of the MoS₂ on HOPG can be used to characterize the edge structure (zig-zag or armchair) of the top graphene layer in HOPG.

In conclusion, the atomically flat MoS₂ surfaces are clean, with a low defect density, and have a typical scale of several micrometers. Moiré patterns are observed due to the lattice mismatch and rotational mis-alignment with the HOPG substrate. Interestingly, imaging of the substrate directly below the MoS₂ layer is shown to be possible, by tuning the tip voltage into the MoS₂ band gap and probing through it to the metallic substrate below. Analyzing moiré patterns in a collection of STM images, we find that there exist at least five different superstructures, and the rotation between the MoS₂ and HOPG lattices tends to have a small value, typically less than 3°. This tendency is consistent with the observed preferred direction of MoS₂ islands as observed on a micrometer scale in our AFM data. Our *ab-initio* calculations indicate that modulation of interlayer interactions between the MoS₂ layer and the graphite substrate are not sufficient to provide the necessary constraint on the orientation of the MoS₂ islands. However, we speculate that the type of graphite step-edge from which the MoS₂ island nucleates and grows predominantly controls the island's lattice orientation. The MoS₂ triangle aligns to the graphite step edge depending on the structure (arm chair or zigzag) of the edge of the uppermost graphene layer. MoS₂ islands growing from zig-zag (or armchair) edges tend to orient with one lattice vector parallel (perpendicular) to the step-edge.

This work was supported in part by the National Science Council of Taiwan through Grant Nos. NSC 101-2112-M-002-024-MY3 and NSC 102-2120-M-002-005.

¹R. A. Bromley, R. B. Murray, and A. D. Yoffe, *J. Phys. C: Solid State Phys.* **5**, 759 (1972).

- ²Th. Böker, R. Severin, A. Müller, C. Janowitz, R. Manzke, D. Voß, P. Krüger, A. Mazur, and J. Pollmann, *Phys. Rev. B* **64**, 235305 (2001).
- ³R. Coehoorn, C. Haas, J. Dijkstra, C. F. J. Flipse, R. A. de Groot, and A. Wold, *Phys. Rev. B* **35**, 6195 (1987).
- ⁴L. F. Mattheiss, *Phys. Rev. B* **8**, 3719 (1973).
- ⁵Z. Tan, H. Tian, T. Feng, L. Zhao, D. Xie, Y. Yang, L. Xiao, J. Wang, T.-L. Ren, and J. Xu, *Appl. Phys. Lett.* **103**, 263506 (2013).
- ⁶B. Sachs, L. Britnell, T. O. Wehling, A. Eckmann, R. Jalil, B. D. Belle, A. I. Lichtenstein, M. I. Katsnelson, and K. S. Novoselov, *Appl. Phys. Lett.* **103**, 251607 (2013).
- ⁷J. Y. Tan, A. Avsar, J. Balakrishnan, G. K. W. Koon, T. Taychatanapat, E. C. T. O'Farrell, K. Watanabe, T. Taniguchi, G. Eda, A. H. Castro Neto, and B. Özyilmaz, *Appl. Phys. Lett.* **104**, 183504 (2014).
- ⁸A. K. Geim and I. V. Grigorieva, *Nature* **499**, 419 (2013).
- ⁹S. Bertolazzi, D. Krasnozhan, and A. Kis, *ACS Nano* **7**, 3246 (2013).
- ¹⁰M. S. Choi, G.-H. Lee, Y.-J. Yu, D.-Y. Lee, S. H. Lee, P. Kim, J. Hone, and W. J. Yoo, *Nat. Commun.* **4**, 1624 (2013).
- ¹¹W. J. Yu, Z. Li, H. Zhou, Y. Chen, Y. Wang, Y. Huang, and X. Duan, *Nat. Mater.* **12**, 246 (2013).
- ¹²Y.-H. Chang, C.-T. Lin, T.-Y. Chen, C.-L. Hsu, Y.-H. Lee, W. Zhang, K.-H. Wei, and L.-J. Li, *Adv. Mater.* **25**, 756 (2013).
- ¹³W. Zhang, C.-P. Chuu, J.-K. Huang, C.-H. Chen, M.-L. Tsai, Y.-H. Chang, C.-T. Liang, Y.-Z. Chen, Y.-L. Chueh, J.-H. He, M.-Y. Chou, and L.-J. Li, *Sci. Rep.* **4**, 3826 (2014).
- ¹⁴P. T. K. Loan, W. Zhang, C.-T. Lin, K.-H. Wei, L.-J. Li, and C.-H. Chen, *Adv. Mater.* **26**, 4838 (2014).
- ¹⁵H. C. Diaz, J. Avila, C. Chen, R. Addou, M. C. Asensio, and M. Batzill, *Nano Lett.* **15**, 1135 (2015).
- ¹⁶Y. Shi, W. Zhou, A.-Y. Lu, W. Fang, Y.-H. Lee, A. L. Hsu, S. M. Kim, K. Kim, H. Y. Yang, L.-J. Li, J.-C. Idrobo, and J. Kong, *Nano Lett.* **12**, 2784 (2012).
- ¹⁷See supplementary material at <http://dx.doi.org/10.1063/1.4919923> for the details of sample preparation, assignment of moiré superstructure unit cells, *ab initio* calculations, and further details.
- ¹⁸Y.-H. Lee, X.-Q. Zhang, W. Zhang, M.-T. Chang, C.-T. Lin, K.-D. Chang, Y.-C. Yu, J. T.-W. Wang, C.-S. Chang, L.-J. Li, and T.-W. Lin, *Adv. Mater.* **24**, 2320 (2012).
- ¹⁹H. C. Diaz, R. Addou, and M. Batzill, *Nanoscale* **6**, 1071 (2014).
- ²⁰C. Zhang, A. Johnson, C.-L. Hsu, L.-J. Li, and C.-K. Shih, *Nano Lett.* **14**, 2443 (2014).
- ²¹J. Kibsgaard, J. V. Lauritsen, E. Lægsgaard, B. S. Clausen, H. Topsøe, and F. Besenbacher, *J. Am. Chem. Soc.* **128**, 13950 (2006).
- ²²C. Ataca, M. Topsakal, E. Aktürk, and S. Ciraci, *J. Phys. Chem. C* **115**, 16354 (2011).
- ²³P. Hohenberg and W. Kohn, *Phys. Rev.* **136**, B864 (1964).
- ²⁴W. Kohn and L. J. Sham, *Phys. Rev.* **140**, A1133 (1965).
- ²⁵D. M. Ceperley and B. J. Alder, *Phys. Rev. Lett.* **45**, 566 (1980).